Vol. 46, No. 3 (2024) 432-446, DOI: 10.24874/ti.1543.09.23.02

Tribology in Industry

www.tribology.rs

RESEARCH

Electro-Mechanical Behavior of Copper-Based Electrical Motor Brushes

Hüseyin İpek[a,b,*], Hamdullah Çuvalcı[a], Tekin Özdemir[c]

[a]*Karadeniz Technical University, Metallurgical and Materials Engineering 61080, Trabzon, Turkey,*
[b]*Karadeniz Technical University, Medical Device Design and Production Application and Research Center 61080, Trabzon, Turkey,*
[c]*National Defense University, Turkish Military Academy, Ankara, Turkey.*

Keywords:

Electric motor brushes
Copper-based brushes
SiC
Graphene
Reinforced composite

* Corresponding author:

Hüseyin İpek
E-mail: hipek@ktu.edu.tr

Received: 11 September 2023
Revised: 21 October 2023
Accepted: 15 February 2024

A B S T R A C T

This study was mainly performed in order to examine the properties of electric motor brushes (EMB). EMBs are electrically conductive and work under wear conditions due to direct contact with the moving part (rotor) of electric motors. In accordance with the scope of the study, EMB characteristics were investigated in two different groups and reproduced with a new technique at the end of this phase. New EMBs were produced via varying proportions of copper matrix, graphene, and silicon carbide reinforcements. The composite-alloy powder elements were carefully squeezed by a cold and single-axis hydraulic press under a pressure of 500 MPa (±5 MPa) following 8 hours of mechanical alloying (MA). The molded composite product (sample) was sintered at 900° C for 1 hour in a reducing gas atmosphere. 100 kPa spring pressure was tested on each sample thrice with 8, 16, 24, and 32 m/s rotational speeds and densities of 4, 8, 12, and 16 A/cm2. Following this process, the electrical conductivity, porosity, hardness, wear loss, surface roughness, and temperature changes were investigated for each sample. It was determined that the electrical conductivity decreased with increasing reinforcement ratio and, in terms of electrical conductivity, affected the brushes' properties negatively.

1. INTRODUCTION

Brushes term comes from the early design of EMBs, composed of bundled copper fibers invented in England about a hundred years ago [1–3]. The primary function of these parts is the polarity of the current flow (transmit the electricity) with a constant pressure, which is called spring pressure [4,5]. Unfortunately, this relatively hardworking condition causes the refill of the brush holders to take a short time due to the wear effect [6]. Nowadays, new studies focus on the improvement of the brushes with high conductivity via spring pressure. In accordance with this purpose, brushes are turned into bulk forms with different components. While materials such as copper and silver assume the electrical

conductivity of the matrix, reinforcing materials such as graphite/graphene (C), hexagonal boron nitride (hBN), molybdenum disulfide (MoS_2), and titanium diboride (TiB_2) are used to increase wear resistance and lubrication properties [7–15].

EMBs are produced by powder metallurgy (PM) techniques and can be classified into two groups: metal-based and graphite-based. Graphite-based brushes are known as carbon brushes. Metal-based EMBs are produced mostly with copper and are called copper brushes. [3,16,17]

Mechanical alloying (MA) is one of the metal-forming processes of PM. The process is a valuable method for producing metal matrix composites (MMCs) [18–20]. MA is a solid-phase powder process technique that involves repeated loops as deformation, welding, and fracture of the powders. Furthermore, almost all the MA processes finalized as nanosized structures exhibit excellent properties and performance compared to conventional coarse-grain materials [18,21–23].

Gr is a one-atom-thick planar sheet (2D) of graphite containing bonded carbon atoms densely packed in a hexagonal crystal lattice at a nanometer scale [24,25]. Gr has been actively explored for future electronic applications capable of a unique combination of mechanical, optical, and electrical properties at one stage [26–30].

Owing to their excellent combination of physical and chemical properties, SiC reinforcement is preferred rather than a carbide ceramic for improving the wear resistance of the composite materials [13,31,32]. Moreover, some properties of SiC may suitably be used in corrosive atmospheres at relatively high temperatures [10].

In present studies, copper-based EMBs were produced by the mechanical alloying method. Reinforcement materials were selected according to their properties. Copper has been chosen as the base element of the matrix because of its excellent electrical and thermal properties. It is also a very suitable material for mechanical alloying. Gr has also been chosen as one of the reinforcement materials due to its electrical and lubricative properties. Finally, SiC has been selected as a secondary reinforcement element to increase hardness and support the structure.

2. EXPERIMENTAL STUDY

2.1 Material compositions and test apparatus

Cu and SiC powders used in the study were obtained from Alfa Aesar and nano-plate Gr powders from Grafen Chemical Industries Co. Pure spherical Cu powder was matrix-maker, Gr as solid lubricant, and SiC was used as reinforcement elements. Composite samples were produced via the mechanical milling method.

Table 1 below depicts the material properties along with the MA parameters used. Figure 1 shows the initial powder morphology of the compositions.

Table 1. MA parameters and powder properties.

Materials	Properties of the materials		MA parameters					
	Powder size	Powder morphology	Explanation	Powder – ball ratio (Ball diameter)	Working speed (rpm)	MA time (h)	Alloying cycle (min)	
							Working	Repose
Cu	37-88 (μm)	Spherical	Matrix	1:5 (10 mm)	400	8	2	1
Gr	50-100 (nm) (Thickness)	Plate (Laminar)	Lubricant and Reinforcement					
SiC	40 (nm)	Irregular	Reinforcement					
Methanol (CH_3OH)	-	Liquid	Liquid Lubricant					

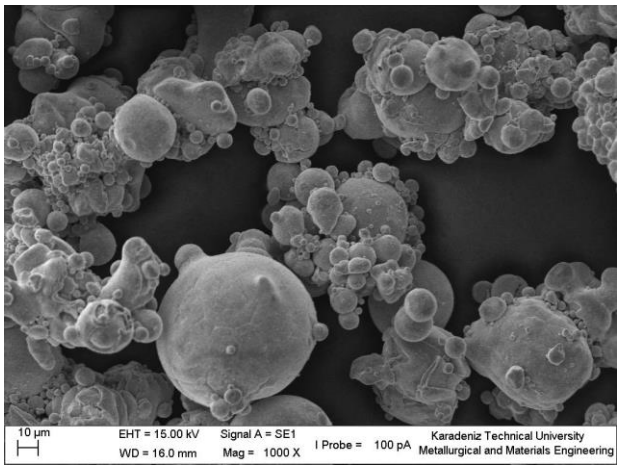

(a)

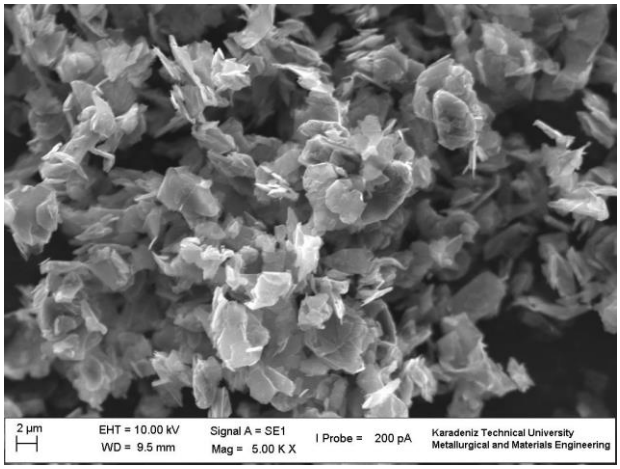

(b)

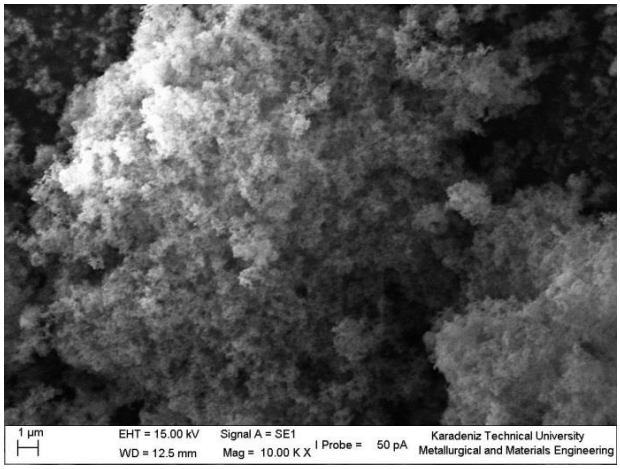

(c)

Fig. 1. SEM imaging of the initial powder morphology (a) Cu powder 1000x, (b) Gr powder 5000x, (c) SiC powder (10000x).

The flow diagram of the experimental process can be seen in Figure 2.

Powders were prepared with precise weighing (0.1 mg precision) and then transferred to the WC (tungsten carbide) bowl for MA. This process was conducted with Retsch PM200, a high-energy planetary mill. To prevent the powder adhesion to the WC bowl, in an amount of wt. 2% methanol added. After the MA process, powders were molded in a single-axis cold press under 500 MPa (±5MPa). Molded samples were sintered for 1 hour at 900° C. A gas mixture (95% nitrogen and 5% hydrogen) sintering atmosphere was used not only to reduce or purify the possible oxidation effects but also to prevent the oxidation of the samples during the sintering phase. The matrix and reinforcement ratios of the samples are shown in Table 2.

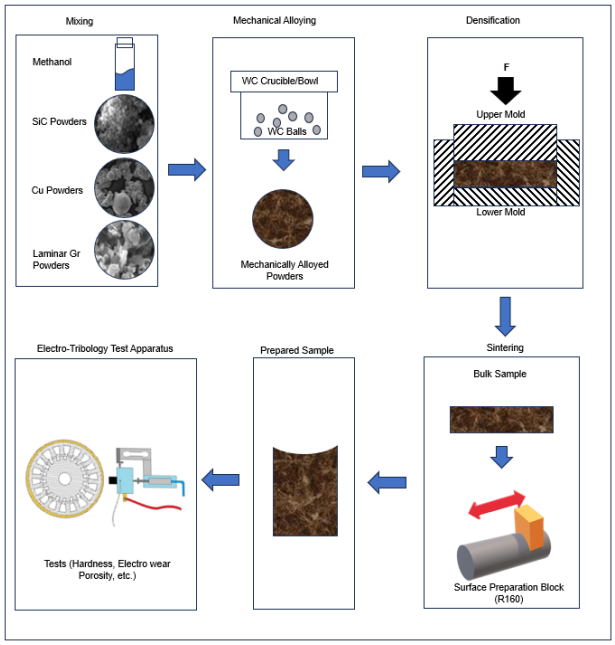

Fig. 2. Flow diagram of the experimental process.

The flat surface of the prepared samples was ground in a suitable radius with 1000-grade sandpaper before the electro-mechanical performance test. Electro-mechanical performance tests were performed via the computer-aided Carbon Brushes Test Ring of Ducom Instruments PVT. LTD. The slip ring of the apparatus was made of pure copper, which has a conductivity of 100% IACS (International Annealed Copper Standard). Samples were subjected to constant rotating speed and spring pressure without electric current for running-in. The test apparatus is modelled schematically, as seen in Figure 3.

Table 2. The composition ratios of the samples.

Sample	Cu (wt. %)	Gr (wt. %)	SiC (wt.%)	Liquid Lubricant (wt. %) (according to the total weight)	Molded Sample Sizes (mm)
5% Gr 0.5% SiC	94.5	5	0.5	2	40 x 20 x 10* (*changeable)
5% Gr 1% SiC	94	5	1		
10% Gr 0.5% SiC	89.5	10	0.5		
10% Gr-1 % SiC	89	10	1		
15% Gr-0.5% SiC	84.5	15	0.5		
15% Gr 01% SiC	84	15	1		

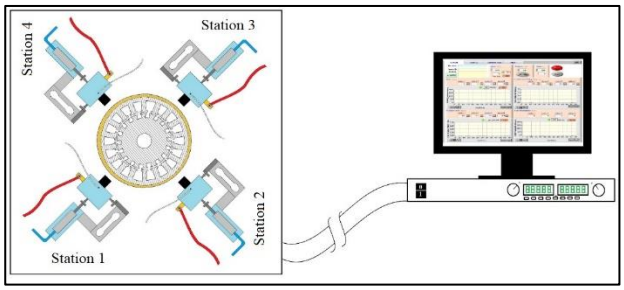

Fig. 3. Electro-tribology wear test apparatus schematically drawing.

The samples were tested only at station 1. Commercial carbon brushes were used at the other stations. This method was employed to ensure the system's stability in terms of pressure and conductivity. All stations except station 1 were calibrated to the commercial carbon brushes, and the working parameters given in Table 3 were applied to all stations. After verifying the system's accuracy (current and voltage settings) with auxiliary equipment, data from station 1 were collected and evaluated. Electro-mechanical performance (in other words, brush life) depends on some parameters. The running-in and experimental parameters can be seen in Table 3.

Table 3. Parameters of the experiments in the electro-tribology test apparatus.

Condition	Current Density (A/cm^2)	Operating Speed (m/s)	Distance (m)	Spring Pressure (kPa)
Experiments	4	8	6650 (±150 m)	100
	8	16		
	12	24		
	16	32		
Running-in	-	10		

3. RESULTS AND DISCUSSIONS

MA process provokes ball-powder-ball collision. This condition causes two effects: (i) cold deformation and (ii) penetration of the reinforcement materials into the matrix. The powders were investigated after the MA process, and their powder form and distribution can be seen in Figure 4.

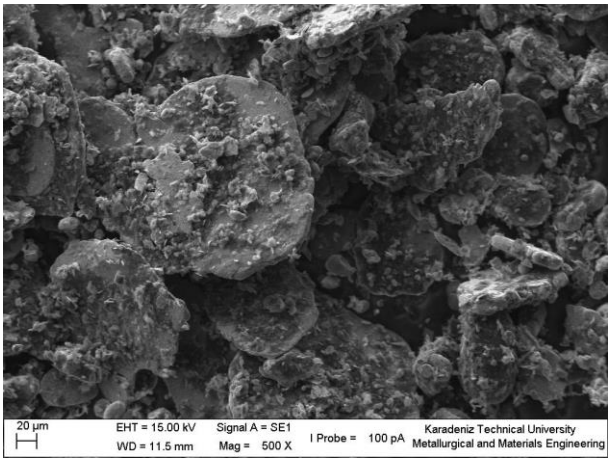

(a)

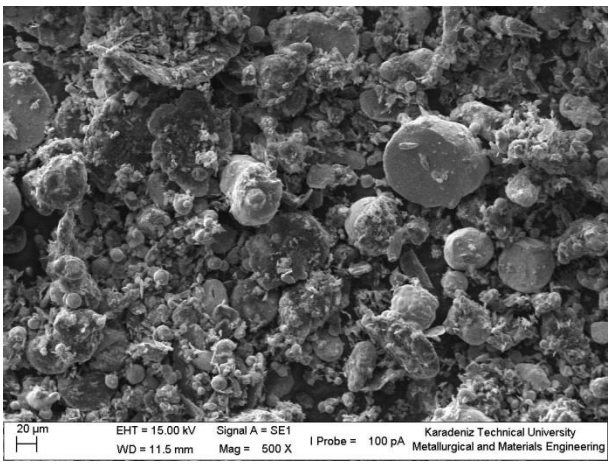

(b)

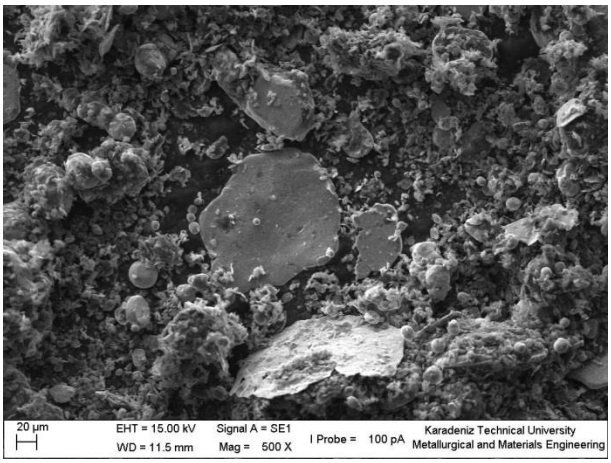

(c)

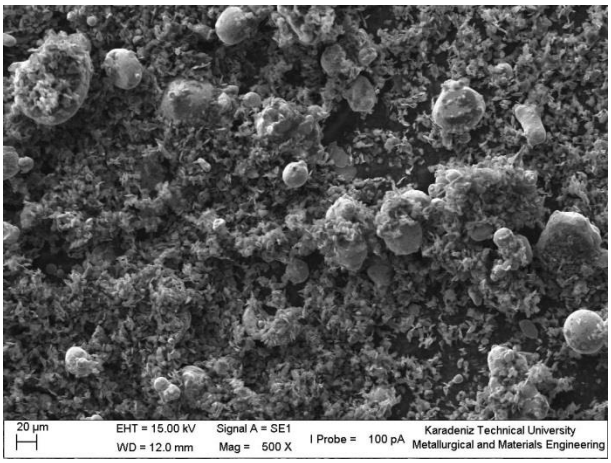

(f)

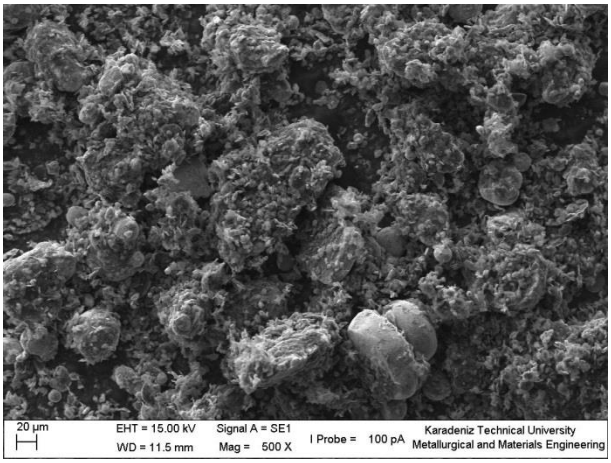

(d)

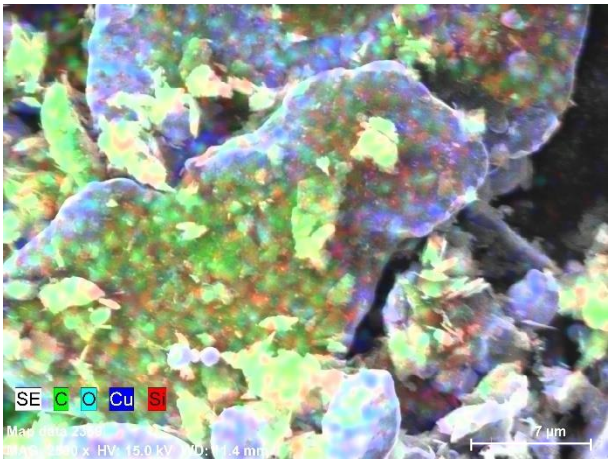

(g)

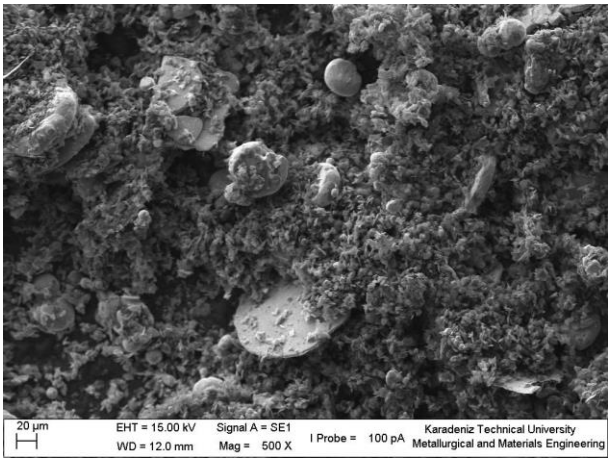

(e)

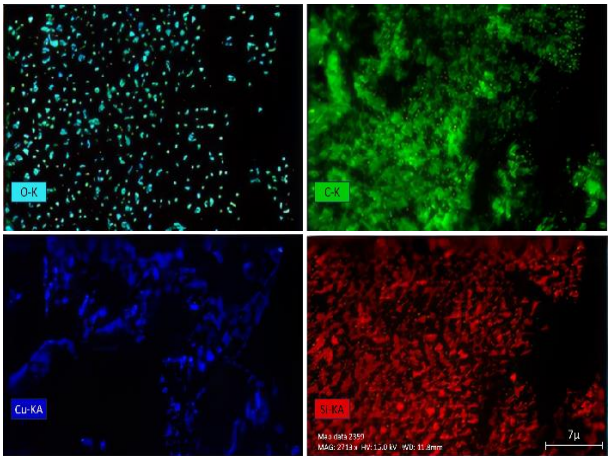

(h)

Fig. 4. SEM images of the sample after 8h MA process (500x) (rest Cu), (a) 5% Gr-0.5% SiC, (b) 5% Gr-1% SiC, (c) 10% Gr-0.5% SiC, (d) 10% Gr-1% SiC, (e) 15% Gr-0.5% SiC, (f) 15% Gr-1% SiC, (g) 5% Gr-1% SiC Mapping applied region, (h) Elemental distribution of (g).

3.1 % Porosity of the samples

The porosity ratios of the produced brush samples were determined according to theoretical density and volume fractions. At first, the weight ratios were converted to volume ratios. The theoretical density and actual densities of each sample were calculated. Second, theoretical and actual densities were converted to % porosity values. Figure 5 shows the % porosity ratio of the samples.

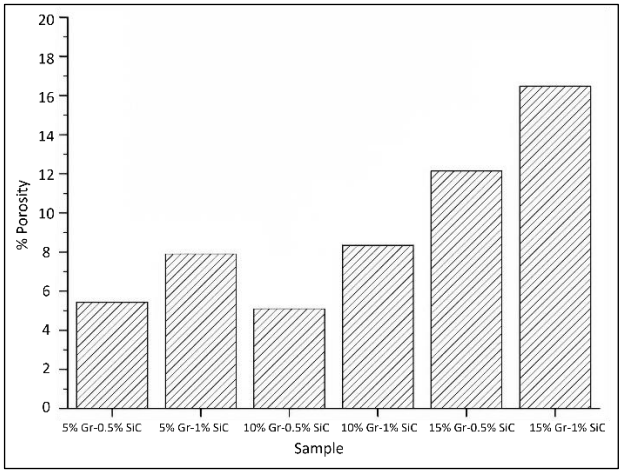

Fig. 5. % porosity of the samples.

As can be seen in Figure 5, the general trend indicates an increase in porosity as the reinforcement ratio rises. It would be appropriate to analyze the graph in segments for a better interpretation. When evaluated based on Gr reinforcement ratios, three main groups can be identified with 5%, 10%, and 15% reinforcement. Within each group, it is observed that an increase in SiC content corresponds to an increase in porosity. This is attributed to the ceramic nature of SiC, which lacks a strong interface with metals. Consequently, this hinders the flow of metals during sintering, leading to a higher formation of porosity. Also, some scientific studies support these findings. Liu et al. (2018) demonstrated increased porosity for Cu-SiC alloys as the SiC content increased. Li et al. (2022) found that Cu-SiC alloys containing SiC exhibited higher porosity values compared to alloys without SiC.

These studies suggest that the effect of SiC on increasing porosity can occur through the following mechanisms:

- SiC increases the surface tension of metals, making it more difficult for metals to bond with each other. This, in turn, hinders the flow of metals during sintering and leads to the formation of more porosity.
- SiC assists in arranging the atoms of metals in a more disorderly manner, allowing metals to come together in a looser fashion.
- SiC expands the gaps between metals, facilitating the formation of porosity.

In the studies' Graphene and SiC Reinforced Cu Composites for High Thermal Conductivity and Electrical Conductivity' by M.A.K. Khan, M.K. Islam, and A.K.M.M.A. Chowdhury, published in Materials & Design, 2022, and 'Porosity and Thermal Conductivity of Graphene-SiC/Cu Composites' by Y. Zhao, Y. Zhang, Y. Zhang, and L. Wang, published in Composites Science and Technology, 2021, researchers investigated the porosity and thermal conductivity of copper composites containing graphite and silicon carbide. They found that an increase in the content of graphite and silicon carbide in the material had a negative impact on porosity.

On the other hand, findings in the literature suggest that graphene has a reducing effect on porosity. Graphene is an excellent lubricant and has a strong interface with metals. These properties reduce the surface tension of metals, facilitating easier bonding between metals, a more orderly arrangement of metal atoms, and a tighter packing of metals. Therefore, the decrease in porosity with 10% Gr reinforcement compared to samples containing 5% Gr is unsurprising. The intriguing part is the unexpected increase in porosity with 15% Gr reinforcement, contrary to the expectation of a decrease. Results obtained from the works of Wang et al. (2022) and Liu et al. (2023) suggest that above a specific threshold, Gr can indeed enhance porosity. This effect is attributed to Gr forming clusters within the material.

As can be seen from Figure 5, the overall trend has been to increase porosity with increasing reinforcement ratio after a total reinforcing ratio of 6% (5% Gr+1%SiC). But an interesting point is the minimum reinforcement content does not have a minimum porosity. The minimum porosity ratio was measured as 5.1 % in the 10 % Gr – 0.5 % SiC labelled sample, and the maximum ratio was measured as 16.5 % in the 15 % Gr – 1 % SiC labelled sample. Porosity is often an undesirable condition in the production of metal matrix composites, adversely affecting many properties. Varol, T. and Çanakçı, A. (2013) highlighted three effective molding (packaging) processes in their study. These stages are presented as follows: (I) sliding and rearrangement of particles, (II) elastic deformation of ductile powders and fragmentation of brittle solids, and (III) plastic deformation [33]. The same study mentioned that particle sliding and rearrangement dominate as the main mechanisms in the first stage of the compression process [33]. The movement of particles is restricted with the increase in pressure, and the energy applied to the powder

compact is generally expended during the fragmentation of the powder and plastic deformation process [34]. Hafizpour, H. R. et al. (2010) stated that the energy expended would manifest itself as a decrease or increase in the porosity ratio during the packing process, depending on the properties of the powders [34]. Yolshina, L.A. and her colleagues (2016) defined the increase in porosity, up to approximately 25% by weight of carbon in the aluminium-carbon system, as high porosity and weak sintering due to the oxide film layer formed by aluminium, a tendency that is also applicable to copper powders, which, like aluminium, tend to form oxide films. Considering these examined studies, the negative impact of copper powders undergoing plastic deformation on packing in the MA process is evident [35]. An increase in the ratio of graphene, a carbon derivative, and the presence of hard ceramic powders lead to adverse and irregular behaviors on porosity, particularly noticeable in the sample with the highest total contribution ratio.

Due to the given reasons, it is difficult to define the effect of SiC on porosity with respect to specimens containing 5% Gr. However, other examples of samples clearly show the effect of the SiC on porosity. When it comes to Gr reinforcement, the porosity values increase with an increasing Gr ratio. The low green density of composites was due to the porosity because compacted composites contain a significant amount of porosity before the sintering process due to nano-plate Gr [36].

On the other hand, green density measurements were employed using the Archimedes method during porosity calculations. It is expected that both the theoretical density and the actual density decrease with an increasing reinforcement ratio. However, in porosity calculations, it has been observed that as the reinforcement ratio increases, there is a deviation from the theoretical density, resulting in higher porosity rates.

3.2 Hardness

Hardness measurements were performed using the Innovatest – Nemesis 9000 automatic hardness test apparatus. The hardness of Brinell was used at a 15.625 kg load with a 2.5 mm diameter indenter ball. The hardness of the samples is given in Figure 6.

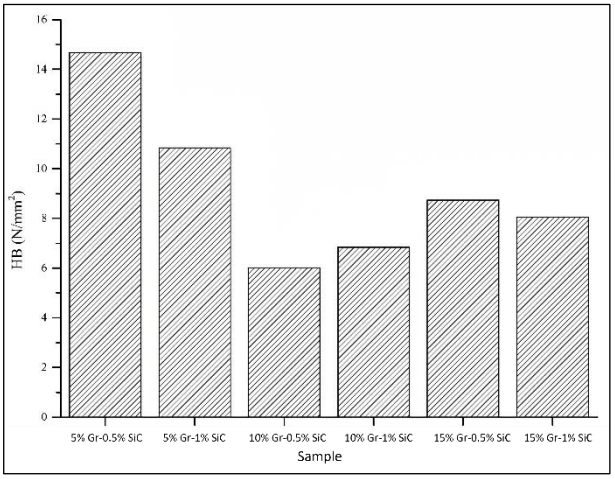

Fig. 6. Brinell hardness of the samples.

The highest hardness value from the 5% Gr – 0.5% SiC coded sample was about 15 HB. The 10%Gr – 0.5% SiC coded sample shows the minimum hardness value; almost half of the first sample was measured. Here, the deformation of the samples during the mechanical alloying/milling stage raises the internal energies of the material, thereby developing a more effective sintering mechanism and causing the sample to soften [12,37].

The highest hardness is observed in samples reinforced with 5% Gr. In this study, when SEM images and porosity rates are examined together, the influence of MA parameters becomes evident. Particle size distribution, porosity, and hardness variations change in parallel for each sample. In the 5% Gr-reinforced sample, it is observed that the solid lubrication property of Gr remains relatively low, and the deformation hardening of Cu particles is observed even after sintering. With a 10% Gr reinforcement, the solid lubrication property becomes more effective, leading to a reduction in the effect of deformation hardening. This effect is also explained by the presence of spherical particles in SEM images (See Figure 4c and d). Thus, a slight decrease in hardness after sintering is expected.

On the other hand, when looking at the 15% Gr-reinforced sample, although the hardness is expected to decrease with an increasing reinforcement ratio, it has increased slightly compared to the 10% Gr-reinforced sample. However, this result is in line with the literature. Studies have shown that increasing reinforcement ratios lead to a decrease in particle size an increase in porosity, and hardness [38].

3.3 Electrical conductivity

The electrical conductivities of the samples were measured by the international annealed copper standard (IACS) with a Fischer Sigmascop device. From the large surfaces of the samples (lower and upper surfaces), a 5-point measurement was taken from random points, the average values were taken, and the conductivity value was found in Figure 4.

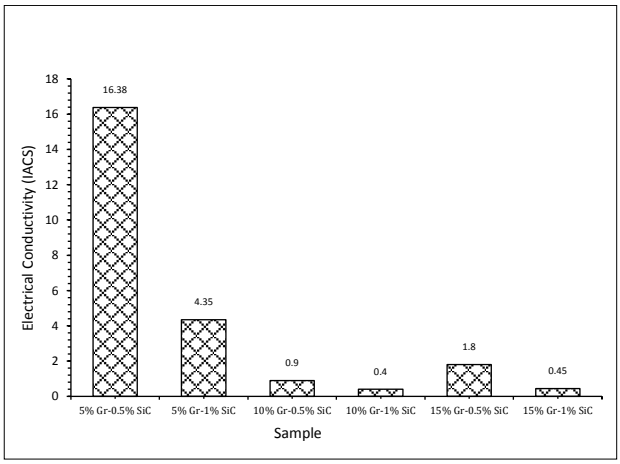

Fig. 7. The electrical conductivity of the samples.

The 5% Gr – 0.5% SiC coded sample showed the highest electrical conductivity value. The electrical conductivity values for this sample were measured as about 16.5 IACS, approximately 4 times higher than the 5% Gr – 1% SiC additive brush samples. The conductivity value of the 5% Gr – 1% SiC coded sample was measured as about 4 IACS. The subsequent samples determined that the electrical conductivity values gradually decreased with the increasing reinforcement ratio, except for the 15% Gr – 0.5% SiC coded sample.

Gr shows good electrical conductivity because of the metallic character in the plane direction. However, electrical conductivity values are inferior between planes due to weak Van der Waals bonds that act between layers [39], and therefore, the increasing Gr ratio electrical conductivity was decreased. This decrease in the conductivity value is also affected by SiC reinforcement, deformation, and the structural increase in porosity. In a study conducted by Bettinali et al. [40], they found a reduction of about 7% in electrical conductivity values at room temperature measurements of pure copper deformed by about 50%. In addition, porosity values increased by more than 30%. Rajkumar and Aravindan [41] have shown that nano graphite particles develop up to 15% electrical conductivity. Again, the conductivities are reduced by reinforcement rates on certain levels, according to the same study. However, contrary to the nano graphite reinforcement Rajkumar and Aravindan [41] used in their study, the brush samples produced with the nano-graphene plate exceeded the 5% reinforcing ratio, and the electrical conductivity value showed a rapid decline. In the present study, this decline was caused by increasing the undirected Gr proportion, SiC reinforcement addition, and distribution of the powders by MA.

3.4 Electro-mechanical behaviors

Electro-mechanical behavior tests were performed with a computer-aided carbon brush test apparatus under different currents and rotating speeds with certain spring pressure. Figure 8 gives the electro-mechanical behaviors of the samples, and optimum operating conditions were determined for each sample. In the study, the rotational speed and current density parameters were simultaneously varied, and the frictional force and voltage drop values were measured. In order to comprehend the correlation indicated by the results, the frictional force - rotational speed graph (blue/circle indicator's lines) and the voltage drop - current density graphs (red/square indicator's lines) are presented on the same coordinate system. The optimum operating conditions term was used for minimum points or intersectional points of friction force and voltage drop.

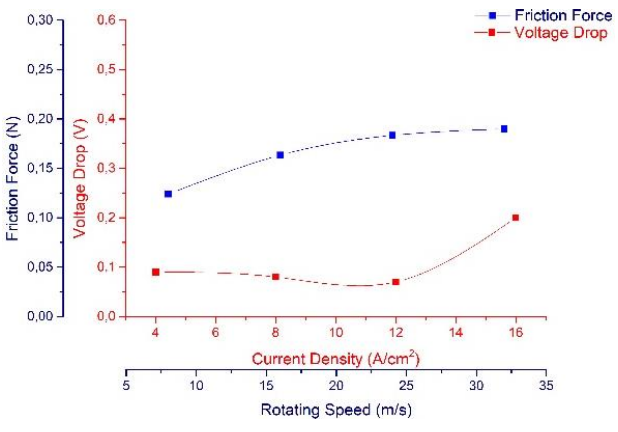

(a)

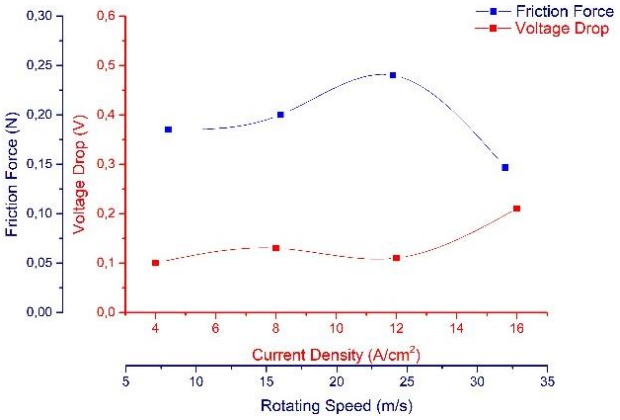

(b)

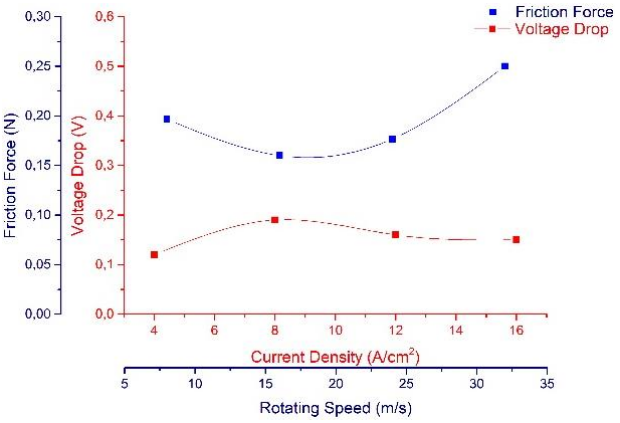

(c)

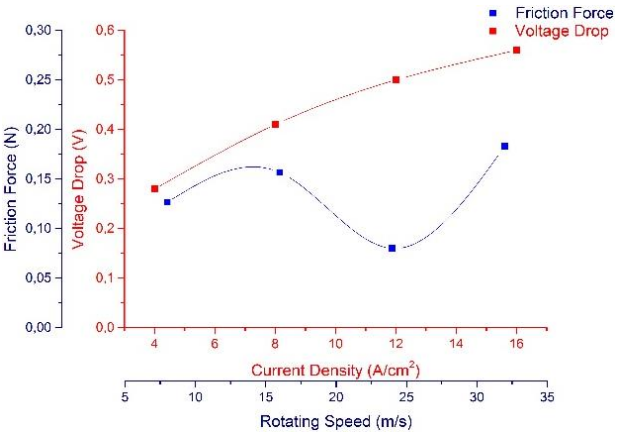

(d)

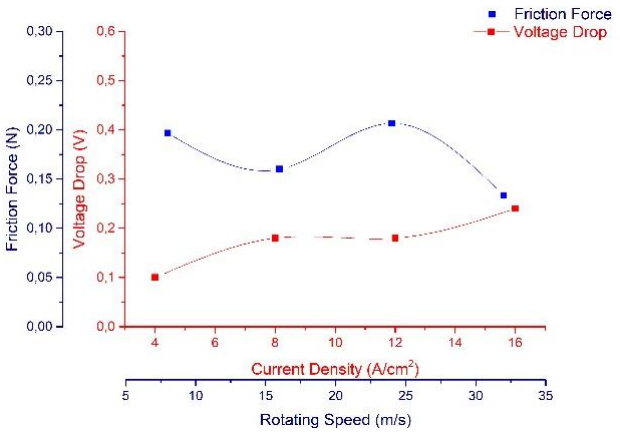

(e)

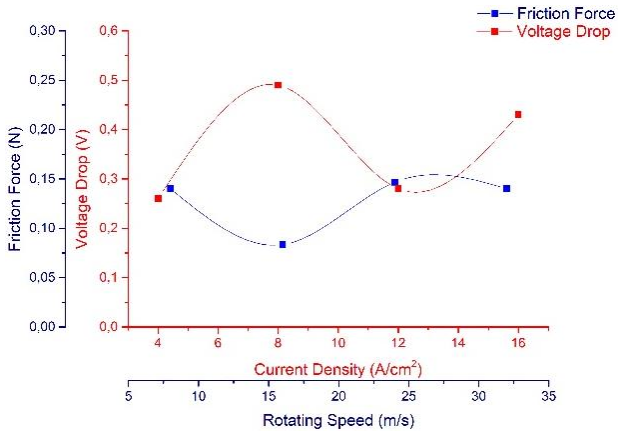

(f)

Fig. 8. Electro-mechanical wear performance of the sample (rest Cu), (a) 5% Gr-0.5% SiC, (b) 5% Gr-1% SiC, (c) 10% Gr-0.5% SiC, (d) 10% Gr-1% SiC, (e) 15% Gr-0.5% SiC, (f) 15% Gr-1% SiC.

It was determined that the frictional force at 5% Gr – 0.5% SiC (Fig. 8-a) reinforced copper brush sample increased step by step and was relatively low with increasing rotation speed. On the other hand, it has been observed that the decrease in voltage has almost the same course with increasing current density up to 16 A/cm². All operating conditions except 16 A/cm² current density and 32 m/s rotating speed were determined as optimum working parameters.

As can be seen from Figure 8-b, the friction force curve with increasing SiC ratio showed a rise to 24 m/s rotating speed. And drop suddenly at 32 m/s to the 0.15 N. However, the voltage drop showed an almost stable value with increasing current density up to 16 A/cm². 4-8 A/cm² current density and 8-6 m/s rotating speed can be evaluated as optimum parameters.

It has been found that in Figure 8-c, the voltage drops show a close value and follow a stable course. It was observed that the friction force increased with the rotation speed increasing from the rotation speed of 16 m/s. The optimal operating parameters for this sample were found to be a working speed of 16 m/s and a current density of 8 A/cm².

Figure 8-d shows that the frictional force increases, and voltage loss increases. Although the frictional force exhibits a relatively unfavourable behavior, the voltage drop was increased with increasing current density. The optimum operating parameters for this brush were determined at 4 A/cm² current density and 8 m/s rotation speeds.

When Figure 8-e is examined, it is seen that the graph form is very similar to the graphic form of the sample containing 5% Gr - 1% SiC. It has been found that the voltage drop value increases slightly with increasing current density, and the friction force generally exhibits unstable behavior. For this sample, it has been determined that the current density of 8 A/cm^2 and the rotation speed of 16 m/s are the optimum working values.

Graph 8-f shows that the voltage drop value shows an irregular trend despite the increasing current density. It has been found that the frictional force exhibits similar values except for the rotation speed value of 16 m/s. It was determined that the optimum working conditions for this sample had rotating speeds of 10 and 20 m/s at current densities of about 5 and 10 A/cm^2, respectively.

When considering all the graphs provided in Figure 8, as a general assessment, it is observed that the voltage drops change inversely with the frictional force (except for Figure 8-d). Additionally, simultaneous variation of current density and rotational speed has resulted in different behaviors for each sample and parameter.

3.5 Scanning electron microscope (SEM) investigations and wear mechanisms

Scanning electron microscopy (SEM) images of the samples were taken from the worn surfaces after the end of all the electro-mechanical tests. Figure 9 and Figure 10 give the wear surface and the elemental distribution of the samples, respectively.

When the surface morphology of Figure 9-a was examined, deep and wide scratches were seen. Besides, some structures can be seen as a layer on the surface. In these findings, it was determined that both abrasive and adhesive wear were the effective wear mechanism of the sample.

When the surface morphology of Figure 9-a was examined, deep and wide scratches were seen. Besides, some structures can be seen as a layer on the surface. In these findings, it was determined that both abrasive and adhesive wear were the effective wear mechanism of the sample.

Figure 9-b shows a very porous surface morphology concerning the sample's low graphene ratio. However, it is seen that porosity ratios with a sample containing 5% Gr - 0.5% SiC have a lower porosity ratio. This structure, where traces of abrasive and adhesive wear are observed, also reveals arc erosion in some regions.

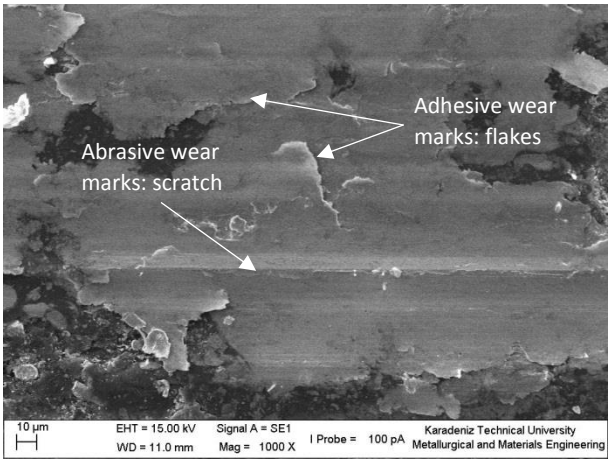

(a)

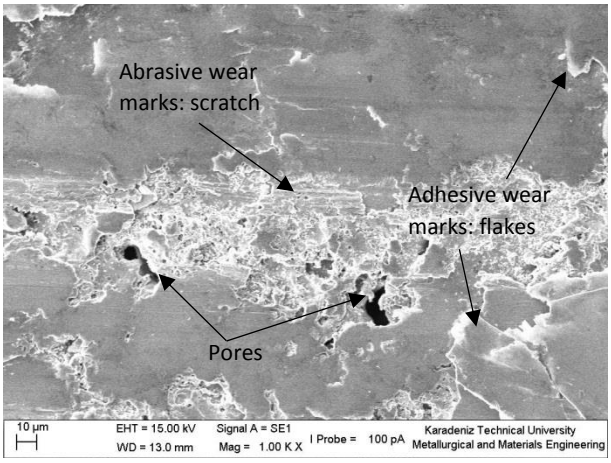

(b)

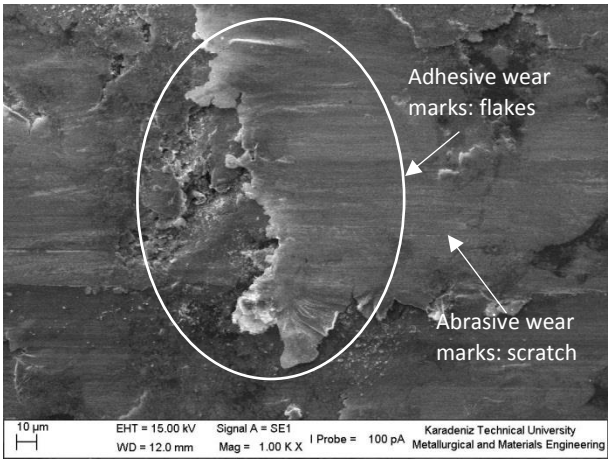

(c)

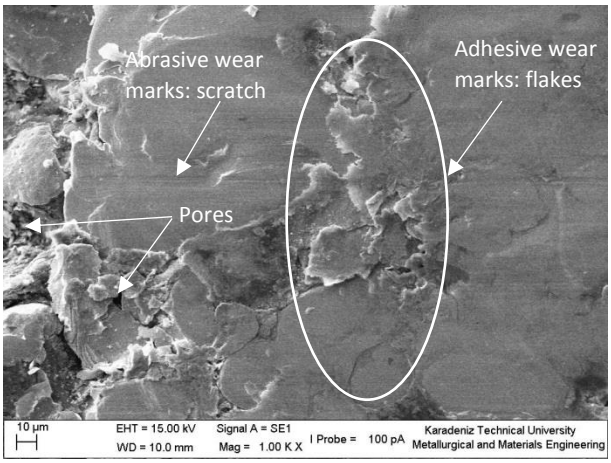

(d)

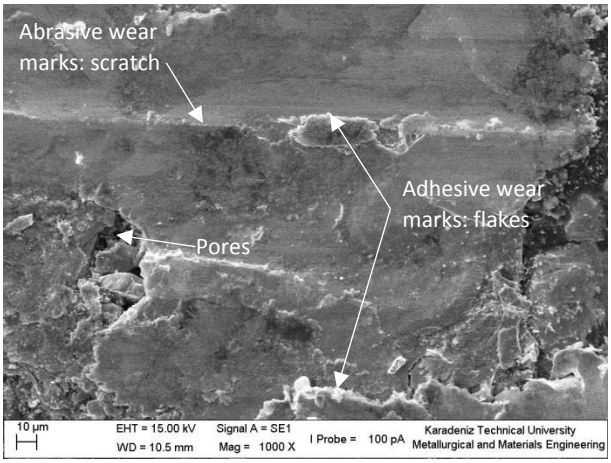

(e)

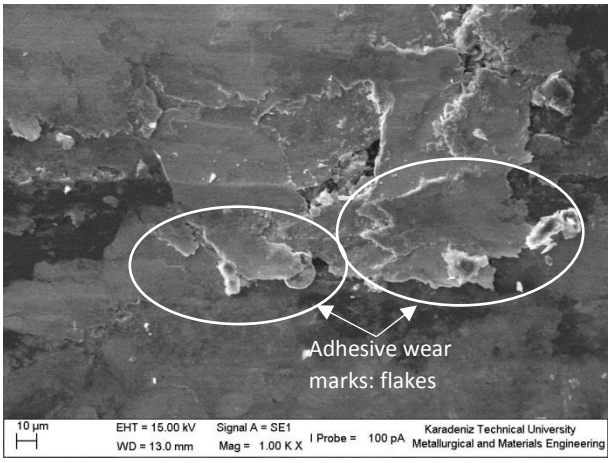

(f)

Fig. 9. SEM images of the wear surface of the samples (rest Cu) (1000x), (a) 5% Gr-0.5% SiC, (b) 5% Gr-1% SiC, (c) 10% Gr-0.5% SiC, (d) 10% Gr-1% SiC, (e) 15% Gr-0.5% SiC, (f) 15% Gr-1% SiC.

In Figure 9-c, a rough surface morphology is remarkable. In addition, the surface has large laminar areas. The surface of the abrasive and adhesive abrasion traces is also found on the surface of the small eruption, indicating arc wear.

The first noticeable feature is that the surface of the sample exhibits a non-sintered surface appearance in Figure 9-d. These regions show relatively thick laminated structures spilling from the surface and where they descend to the lower layer. The weight loss graph in Figure 10 shows that the results are consistent if we consider that the most wear is seen in this sample. It is also seen that the surface of the laminated structures, which have deep scratches on the surface and are separated, tends to be covered.

In Figure 9-e, the effect of increasing graphene on the surface of the sample is noticeable. Referring to the graph of hardness given in Figure 6, it can be seen that the hardness value is slightly increased compared to the previous sample. This situation has been found to cause a visible decrease in the areas of surface debris. Although laminated structures showing adhesive traces of wear are present in surface morphology, dense and partially deep scratches, indicate that the dominant wear mechanism is abrasive wear.

As the ratio of graphene and SiC increases, regional spills are seen in relatively large proportions compared to the previous sample in Figure 9-f. It has been found that the abrasive wear mechanism is the abrasion mechanism for this sample.

When SEM images are examined, both abrasive and adhesive wear traces are observed on all wear surfaces. On the other hand, an increased graphene ratio is seen to be the active mechanism in adhesive wear. Due to the low levels of SiC reinforcement used as a ratio, it has been determined that the abrasive wear traces have occurred in the form of fine scratches. The effect of SiC on the composite material has been examined in more detail under the heading of hardness.

In examining wear surfaces, discussing similar mechanisms for all samples is possible. However, another important aspect that needs to be addressed here is fatigue, lubricating film, and plastic deformation. Upon careful examination of the surfaces, it will be observed that almost the entire surface of each sample has a flake structure ready to peel off. These flake structures indicate superficial plastic deformation. This situation suggests that fatigue occurs on the surfaces due to the friction effect, and after a while, they will

detach and peel off from the surface. However, the relatively low weight loss (see Fig. 11) indicates the involvement of another mechanism. This mechanism is commonly encountered, especially in moving systems containing lubricants (here, graphene as a solid lubricant) [42]. Thus, both the sample surface and the counter surface are protected, and the service life of the material is extended.

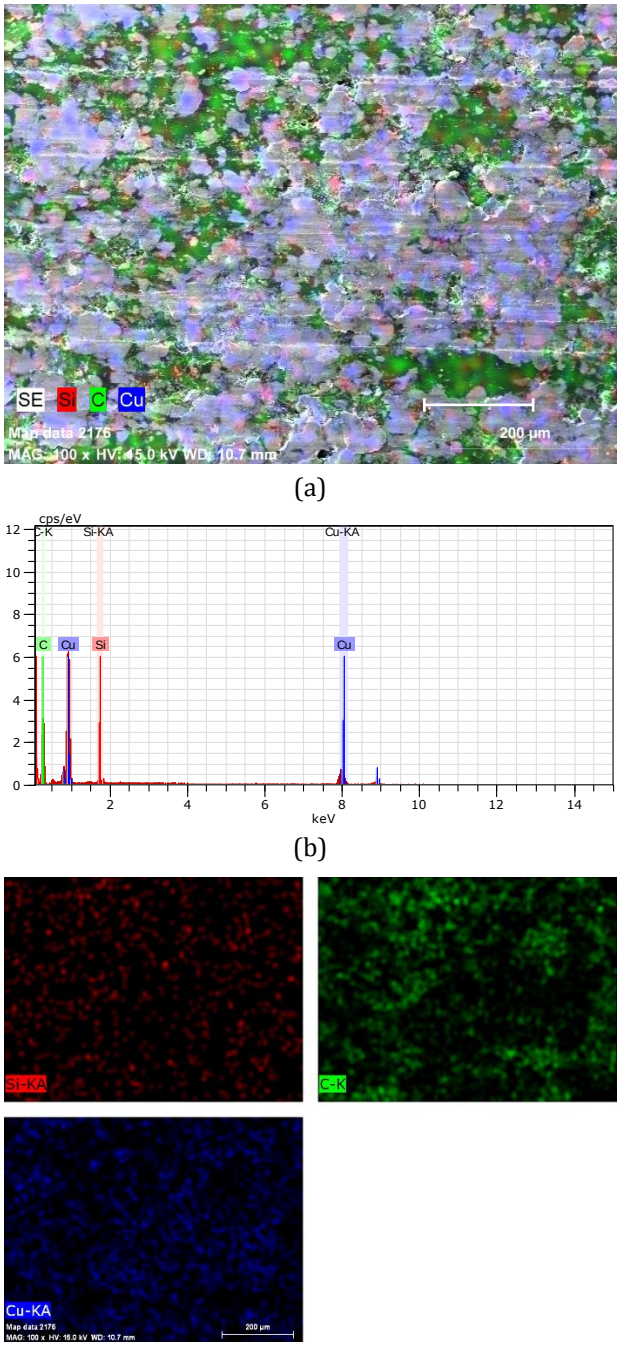

Fig. 10. Elemental distribution of the 15% Gr-0.5% SiC bulk sample (EDS analysis-mapping method) (a) Elemental distribution of the sample, (b) Elemental analysis,(c) Mapping applied region.

In addition, studies indicate that using reinforcement elements with high hardness increases the wear resistance of structures [41-45]. This study shows that despite the low ratio of SiC reinforcement used, it plays a role in this effect. It has demonstrated its influence in preserving the structural integrity of the flakes on the surface and has contributed to the relatively low weight loss.

Figure 10 provides an example illustrating the elemental distribution of a bulk sample. A homogeneous distribution is observed When examining the image obtained through mapping techniques (Figure 10-c).

3.6. Weight loss

The weight loss of the samples was measured with a high precision (0,1 mg) balance. The weight loss of the samples after electro-mechanical wear tests can be seen in Figure 11. The points on the graph show the weight loss of the sample after the test with the given parameters, while the total weight loss shows the sum of the weights of one sample lost in all the parameters.

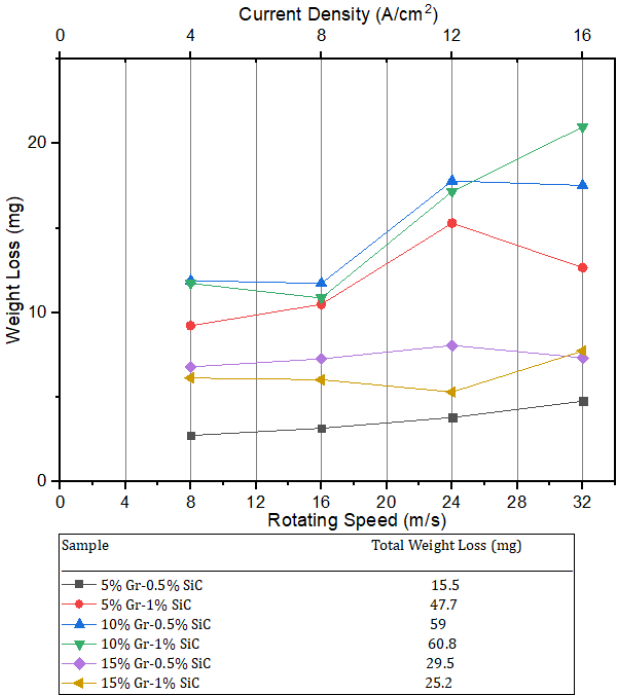

Fig. 11. Weight loss of the samples.

According to Figure 11, the sample with the least weight loss was found to be the sample containing 5% Gr-0.5% SiC. This condition can be explained by the hardness of the sample. The hardest sample should represent minimum wear. With the

increasing Gr content, wear loss increased up to 15 wt %. As the ratios of SiC and Gr increased, it was observed that the total wear loss increased up to samples containing 15% Gr. This trend is approximately proportional to the change in porosity. However, when examining samples containing 15% Gr, it can be observed that the total wear loss tends to decrease suddenly. This is attributed to both the effective mechanism of the increased graphene ratio in reducing wear losses due to its solid lubricating properties and the change in powder morphology according to the MA parameters. When examining the SEM evaluations of powder morphologies after AM given in Figure 4, it is evident that as the copper powder content capable of reaching a flake structure increases, the wear losses of compositions also decrease. On the other hand, agglomeration is another phenomenon commonly encountered in such studies. The agglomeration effect can be seen at lower nanoparticle addition. However, the MA process could reduce the agglomeration of the powders to a certain level, and all progress could be changed with higher reinforcement content. In the case of agglomeration, it is necessary to evaluate the hardness, porosity, lubrication property, and MA parameters of the material, taking these factors into consideration.

4. CONCLUSION

The samples were produced and investigated with the given parameters in Table 2 and Table 3, respectively. According to the investigation of the brushes, the following conclusions were found;

- Increasing the Gr ratio and distributed Gr powders (undirected) by MA, resulting in reduced electrical conductivity of the reinforced brush samples.
- Generally, the voltage drop behavior of the brush tended to increase with increasing current density and rotation speed, although there were deviations in some operating conditions.
- It was determined that friction force values showed different attitudes and did not fit a certain schema in different working conditions.
- According to Brinell hardness values, the highest hardness was found to be 5 % Cu - 0.5 % SiC brush. This situation is also reflected in the weight loss graph. The lowest weight loss in total was found in the same sample.
- The layered structure of the graphene caused the dominant wear mechanism to change from abrasive wear to adhesive wear in the copper-based brush with an increasing Gr ratio.

The MA parameters used in this study were implemented with fixed parameters identified in the preliminary work. It is considered beneficial to improve the sintering mechanism, reduce porosity rates, and enhance the electrical conductivity of the samples to determine these parameters separately for each composition, carry out production in this manner, and conduct tests.

Acknowledgement

This study was supported by the Scientific Research Projects Unit of Karadeniz Technical University with project no. FHD-2016-5709

We would like to give a special thanks to Lect. Enis OĞUZ from Middle East Technical University for editing and proofreading.

ORCID iDs

Hüseyin İpek 0000-0003-0835-2978
Hamdullah Çuvalcı 0000-0002-8257-8310
Tekin Özdemir 0000-0001-6843-4014

REFERENCES

[1] J. Xia, Z. Hu, Z. Chen, and G.-Y. Ding, "Preparation of carbon brushes with thermosetting resin binder," *Transactions of Nonferrous Metals Society of China*, vol. 17, no. 6, pp. 1379–1384, Dec. 2007, doi: 10.1016/s1003-6326(07)60281-7.

[2] N. Argibay and W. G. Sawyer, "Low wear metal sliding electrical contacts at high current density," *Wear*, vol. 274–275, pp. 229–237, Jan. 2012, doi: 10.1016/j.wear.2011.09.003.

[3] P. G. Slade. (2017, Jan. 31). *Electrical contacts* [Online]. Available: doi: 10.1201/b15640.

[4] N. Argibay, J. A. Bares, and W. G. Sawyer, "Asymmetric wear behavior of self-mated copper fiber brush and slip-ring sliding electrical contacts in a humid carbon dioxide environment," *Wear*, vol. 268, no. 3–4, pp. 455–463, Feb. 2010, doi: 10.1016/j.wear.2009.08.036.

[5] M. Freschi et al., "Investigation of second phase concentration effects on tribological and electrical properties of Cu–WS2 composites," *Tribology International*, vol. 166, p. 107357, Feb. 2022, doi: 10.1016/j.triboint.2021.107357.

[6] Y. A. Wang, J. X. Li, Y. Yan, and L. Qiao, "Effect of surface film on sliding friction and wear of copper-impregnated metallized carbon against a Cu–Cr–Zr alloy," *Applied Surface Science*, vol. 258, no. 7, pp. 2362–2367, Jan. 2012, doi: 10.1016/j.apsusc.2011.10.030.

[7] G. Qian, Y. Feng, B. Li, S. Huang, H. Liu, and K. Ding, "Effect of electrical current on the tribological behavior of the Cu-WS2-G composites in air and vacuum," *Chinese Journal of Mechanical Engineering*, vol. 26, no. 2, pp. 384–392, Mar. 2013, doi: 10.3901/cjme.2013.02.384.

[8] B. Wu, B. Xu, B. Zhang, and Y. Lu, "Preparation and properties of Ni/nano-Al2O3 composite coatings by automatic brush plating," *Surface & Coatings Technology*, vol. 201, no. 16–17, pp. 6933–6939, May 2007, doi: 10.1016/j.surfcoat.2006.12.022.

[9] M. Lopez, D. Corredor, C. Camurri, V. Vergara, and J. A. Jimenez, "Performance and characterization of dispersion strengthened Cu–TiB2 composite for electrical use," *Materials Characterization*, vol. 55, no. 4–5, pp. 252–262, Nov. 2005, doi: 10.1016/j.matchar.2005.04.006.

[10] A. Motealleh, A. L. Ortiz, O. Borrero-Lopez, and F. Guiberteau, "Effect of hexagonal-BN additions on the sliding-wear resistance of fine-grained α-SiC densified with Y3Al5O12 liquid phase by spark-plasma sintering," *Journal of the European Ceramic Society*, vol. 34, no. 3, pp. 565–574, Mar. 2014, doi: 10.1016/j.jeurceramsoc.2013.09.016.

[11] R. Beiranvand and S. Valedbagi, "Electronic and optical properties of h-BN nanosheet: A first principles calculation," *Diamond and Related Materials*, vol. 58, pp. 190–195, Sep. 2015, doi: 10.1016/j.diamond.2015.07.008.

[12] S. Mahdavi and F. Akhlaghi, "Effect of the graphite content on the tribological behavior of AL/GR and AL/30SIC/GR composites processed by in situ Powder Metallurgy (IPM) method," *Tribology Letters*, vol. 44, no. 1, pp. 1–12, Jul. 2011, doi: 10.1007/s11249-011-9818-2.

[13] R. Sedlák et al., "Effect of graphene platelets on tribological properties of boron carbide ceramic composites," *International Journal of Refractory Metals & Hard Materials*, vol. 65, pp. 57–63, Jun. 2017, doi: 10.1016/j.ijrmhm.2016.11.015.

[14] W. Qu et al., "Copper matrix composites reinforced by three-dimensional netlike graphene towards enhanced mechanical property and wear resistance," *Composites Communications*, vol. 32, p. 101187, Jun. 2022, doi: 10.1016/j.coco.2022.101187.

[15] M. Wu, Z. Chen, C. Huang, K. Huang, K. Jiang, and L. Jian, "Graphene platelet reinforced copper composites for improved tribological and thermal properties," *RSC Advances*, vol. 9, no. 68, pp. 39883–39892, Jan. 2019, doi: 10.1039/c9ra07962a.

[16] Q. Hongling et al., "Tribological performance of Carbon Brush/Collector ring for hydroelectric generator under dry sliding condition with Current-Carrying and without Current-Carrying," *Tribology*, vol. 39, no. 6, pp. 713–722, 2019, doi: 10.16078/j.tribology.2019114.

[17] R. Shakarappa, A. A. Peter, M. V. Mallikarjuna, S. Padmanabhan, and P. Ramesha, "Synthesis, Microstructure and Wear Analysis of Copper Alloy with Alumina and Graphene as Reinforcement," *International Journal of Vehicle Structures & Systems*, vol. 14, no. 3, Jun. 2022, doi: 10.4273/ijvss.14.3.16.

[18] A. Çanakçı, T. Varol, H. Çuvalcı, F. Erdemir, S. Özkaya, and E. D. Yalçin, "Synthesis of novel CuSn 10 -graphite nanocomposite powders by mechanical alloying," *Micro & Nano Letters*, vol. 9, no. 2, pp. 109–112, Feb. 2014, doi: 10.1049/mnl.2013.0715.

[19] C. Suryanarayana, "Mechanical alloying: a critical review," *Materials Research Letters*, vol. 10, no. 10, pp. 619–647, May 2022, doi: 10.1080/21663831.2022.2075243.

[20] S. Rajendrachari, "An overview of High-Entropy alloys prepared by mechanical alloying followed by the characterization of their microstructure and various properties," *Alloys*, vol. 1, no. 2, pp. 116–134, Jun. 2022, doi: 10.3390/alloys10 2008.

[21] M. Tavoosi, F. Karimzadeh, and M. H. Enayati, "Fabrication of Al–Zn/α-Al2O3 nanocomposite by mechanical alloying," *Materials Letters*, vol. 62, no. 2, pp. 282–285, Jan. 2008, doi: 10.1016/j.matlet.2007.05.017.

[22] M. Vaidya, G. M. Muralikrishna, and B. S. Murty, "High-entropy alloys by mechanical alloying: A review," *Journal of Materials Research*, vol. 34, no. 5, pp. 664–686, Mar. 2019, doi: 10.1557/jmr.2019.37.

[23] C. Shuai et al., "Mechanical alloying of immiscible metallic systems: process, microstructure, and mechanism," *Advanced Engineering Materials*, vol. 23, no. 4, Feb. 2021, doi: 10.1002/adem.202001098.

[24] W. Choi, I. Lahiri, R. Seelaboyina, and Y. S. Kang, "Synthesis of Graphene and its applications: a review," *Critical Reviews in Solid State and Materials Sciences*, vol. 35, no. 1, pp. 52–71, Feb. 2010, doi: 10.1080/10408430903505036.

[25] Y. Wang, S. Li, H. Yang, and J. Luo, "Progress in the functional modification of graphene/graphene oxide: a review," *RSC Advances*, vol. 10, no. 26, pp. 15328–15345, Jan. 2020, doi: 10.1039/d0ra01068e.

[26] S. A. Han et al., "Hexagonal boron nitride assisted growth of stoichiometric Al 2 O 3 dielectric on graphene for triboelectric nanogenerators," *Nano Energy*, vol. 12, pp. 556–566, Mar. 2015, doi: 10.1016/j.nanoen.2015.01.030.

[27] M. Taghioskoui, "Trends in graphene research," *Materials Today*, vol. 12, no. 10, pp. 34–37, Oct. 2009, doi: 10.1016/s1369-7021(09)70274-3.

[28] C. Oshima and A. Nagashima, "Ultra-thin epitaxial films of graphite and hexagonal boron nitride on solid surfaces," *Journal of Physics: Condensed Matter*, vol. 9, no. 1, pp. 1–20, Jan. 1997, doi: 10.1088/0953-8984/9/1/004.

[29] S. F. Bartolucci et al., "Graphene–aluminum nanocomposites," *Materials Science and Engineering: A*, vol. 528, no. 27, pp. 7933–7937, Oct. 2011, doi: 10.1016/j.msea.2011.07.043.

[30] S. K. Tiwari, S. Sahoo, N. Wang, and A. Huczko, "Graphene research and their outputs: Status and prospect," *Journal of Science: Advanced Materials and Devices*, vol. 5, no. 1, pp. 10–29, Mar. 2020, doi: 10.1016/j.jsamd.2020.01.006.

[31] Y. Zou, C. Tan, Z. Qiu, W. Ma, K. Min, and D. Zeng, "Additively manufactured SiC-reinforced stainless steel with excellent strength and wear resistance," *Additive Manufacturing*, vol. 41, p. 101971, May 2021, doi: 10.1016/j.addma.2021.101971.

[32] M. Uthayakumar, S. Aravindan, and K. Rajkumar, "Wear performance of Al–SiC–B4C hybrid composites under dry sliding conditions," *Materials in Engineering*, vol. 47, pp. 456–464, May 2013, doi: 10.1016/j.matdes.2012.11.059.

[33] T. Varol and A. Çanakçı, "Effect of particle size and ratio of B4C reinforcement on properties and morphology of nanocrystalline Al2024-B4C composite powders," *Powder Technology*, vol. 246, pp. 462–472, Sep. 2013, doi: 10.1016/j.powtec.2013.05.048.

[34] H. R. Hafizpour, A. Simchi, and S. Parvizi, "Analysis of the compaction behavior of Al–SiC nanocomposites using linear and non-linear compaction equations," *Advanced Powder Technology*, vol. 21, no. 3, pp. 273–278, May 2010, doi: 10.1016/j.apt.2009.12.003.

[35] L. A. Yolshina, R. V. Muradymov, I. V. Korsun, G. A. Yakovlev, and C. B. Smirnov, "Novel aluminum-graphene and aluminum-graphite metallic composite materials: Synthesis and properties," *Journal of Alloys and Compounds*, vol. 663, pp. 449–459, Apr. 2016, doi: 10.1016/j.jallcom.2015.12.084.

[36] T. Varol and A. Çanakçı, "An investigation on wear behavior of Cu-graphite nanocomposites prepared by flake powder metallurgy," *Industrial Lubrication and Tribology*, vol. 69, no. 1, pp. 8–14, Jan. 2017, doi: 10.1108/ilt-11-2015-0187.

[37] Md. A. Islam and Z. Farhat, "Effect of porosity on dry sliding wear of Al–Si alloys," *Tribology International*, vol. 44, no. 4, pp. 498–504, Apr. 2011, doi: 10.1016/j.triboint.2010.12.007.

[38] E. B. Moustafa and M. A. Taha, "Preparation of high strength graphene reinforced Cu-based nanocomposites via mechanical alloying method: microstructural, mechanical and electrical properties," *Applied Physics A*, vol. 126, no. 3, Feb. 2020, doi: 10.1007/s00339-020-3412-0.

[39] V. Georgakilas. (2014, Mar. 21). *Functionalization of Graphene* [Online]. Available: doi: 10.1002/9783527672790.

[40] L. Bettinali, S. Tosti, and A. Pizzuto, "Mechanical and electrical properties of cryo-worked CU," *Journal of Low Temperature Physics*, vol. 174, no. 1–2, pp. 64–75, Oct. 2013, doi: 10.1007/s10909-013-0913-7.

[41] K. Rajkumar and S. Aravindan, "Tribological behavior of microwave processed copper–nanographite composites," *Tribology International*, vol. 57, pp. 282–296, Jan. 2013, doi: 10.1016/j.triboint.2012.06.023.

[42] S. Arif, A. Samad, H. Hadidi, M. B. N. Shaikh, and S. Ansari, "Dry sliding wear investigation of graphene reinforced copper-silica sand composite by response surface methodology," *Materials Today Communications*, vol. 33, p. 104857, Dec. 2022, doi: 10.1016/j.mtcomm.2022.104857.

[43] N. Nemati, R. A. Khosroshahi, M. Emamy, and A. Zolriasatein, "Investigation of microstructure, hardness and wear properties of Al–4.5wt.% Cu–TiC nanocomposites produced by mechanical milling," *Materials in Engineering*, vol. 32, no. 7, pp. 3718–3729, Aug. 2011, doi: 10.1016/j.matdes.2011.03.056.

[44] P. Jha, R. K. Gautam, R. Tyagi, and D. Kumar, "Sliding Wear Behavior of TiC-Reinforced Cu-4 wt.% Ni Matrix Composites," *Journal of Materials Engineering and Performance*, vol. 25, no. 10, pp. 4210–4218, Aug. 2016, doi: 10.1007/s11665-016-2303-1.

[45] S. C. Tjong and K. C. Lau, "Properties and abrasive wear of TiB 2 /Al-4%Cu composites produced by hot isostatic pressing," *Composites Science and Technology*, vol. 59, no. 13, pp. 2005–2013, Oct. 1999, doi: 10.1016/s0266-3538(99)00056-1.

[46] A. Kumar, P. K. Jha, and M. M. Mahapatra, "Abrasive Wear Behavior of In Situ TiC Reinforced with Al-4.5%Cu Matrix," *Journal of Materials Engineering and Performance*, vol. 23, no. 3, pp. 743–752, Jan. 2014, doi: 10.1007/s11665-013-0836-0.